Porosity and lithology prediction at Caballos Formation in the Puerto Colón Oil Field in Putumayo (Colombia)

Horacio Acevedo, Ecopetrol, Bogotá, Colombia
Wayne D. Pennington, Michigan Technological University, Houghton, Michigan, U.S.

At a given pressure and temperature, differences in the velocities of propagation of P- and S-waves in rocks can indicate differences in various properties of the rocks, including porosity, lithological composition, and the fluids occupying the pore space. In the absence of direct S-wave observations, we study the response of interfaces between rock units to wavefronts with different angles of incidence to infer changes in S-wave velocities. We have used modern techniques of seismic inversion that involve P- and S-impedance estimation from various angle stacks to estimate the rock properties.

This study presents the results of a seismic inversion analysis and interpretation of the Acae-3D seismic volume. The main target is the higher-quality areas of Caballos Formation at Puerto Colón oil field in the foreland of Columbia's Putumayo Basin (Figure 1). The oil field is a faulted anticline or monocline with regional dip (Figure 2). The study was based on 3D angle-dependent seismic data and well-log information, which were used to obtain P-impedance (PI) and S-impedance (SI) response. The log data available was of mixed quality due to poor borehole conditions. As a result, this study used existing rock physics models and extreme well-log editing to create suites of highly corrected logs, including modeled V_S logs, for inversion and interpretation.

Caballos Formation (Aptian-Albian) is mostly a sequence of sandstones, interbedded with dark gray shales with thin coal laminations. The mean thickness is 250 ft and average porosity in the sands is 12%. This sequence represents the initiation of the Cretaceous sedimentation in a transgressive deltaic environment over Jurassic volcano-sediments. Figure 3 shows more details of the stratigraphic sequence.

Puerto Colón, discovered by Texaco in the late 1960s, is at a depth of 10 500 ft. The field has produced 31 million barrels of 30.5° API oil. A large difference between the reservoir pressure (4300 psi, almost constant since the discovery due to a strong water drive) and the bubble pressure of the oil (1600 psi) implies that a free gas phase is unlikely to ever be present in the field. This fact and the low GOR of 458 SCF/STB makes oil and water indistinguishable using seismic observations, thus limiting the study to the characterization of the solid fraction of the rocks (porosity and lithology).

Seismic and well data. The Acae 3D seismic volume was recorded by Ecopetrol in 2000 in an effort to identify additional high-quality areas. The seismic data are 36 fold within 20 × 40 m bins, with good offset distribution and narrow azimuthal range. Data from preprocessed CDP gathers in an area covering 31 km^2 (Figure 4) were separated into four overlapping angle-dependent gathers, (0-20°; 10-25°; 20-35°; and 25-40°). These gathers were independently stacked, migrated, and aligned, to produce four angle-stack seismic volumes (ASVs). The different ASVs show similar phase and frequency content, but the amplitude differences with offset can be seen in the angle-dependent gathers and in the spectra of Figure 5. The seismic data are, in general, good quality data.

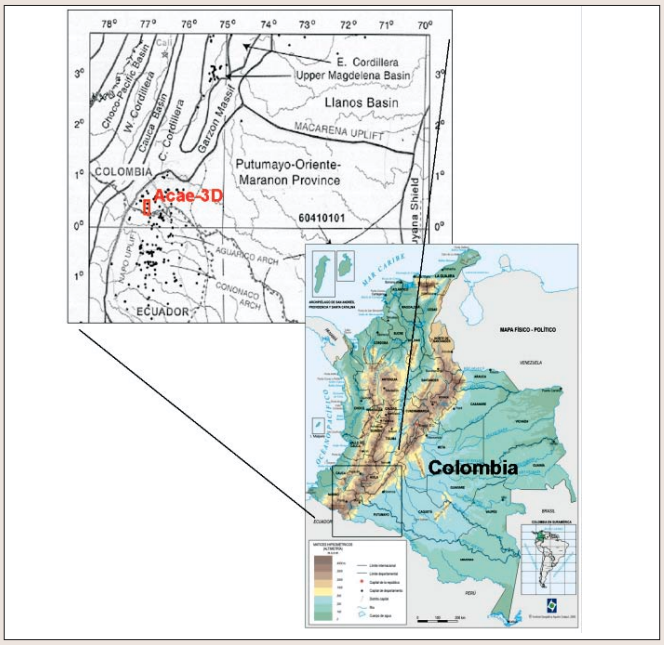

Figure 1. *Location of the Acae 3D seismic volume. (Modified from Higley, 2001.)*

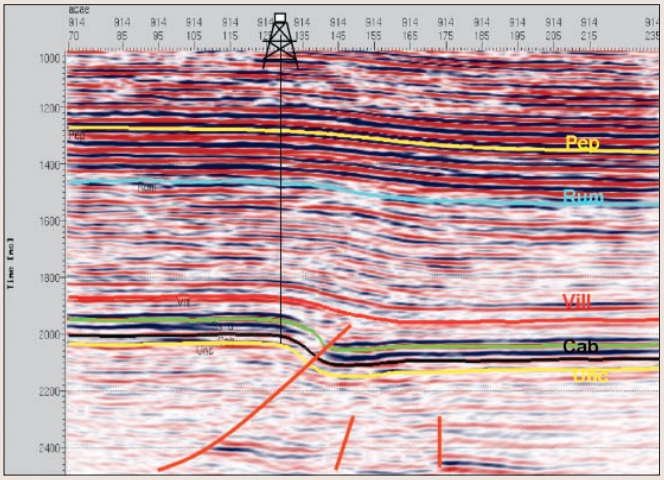

Figure 2. *Geologic model along a dip section at Puerto Colon Oil Field and the interpreted horizons.*

Well-log data must be used together with seismic data for deterministic inversion and interpretation in terms of rock quality or lithology. Well-log measurements of P-velocity (from DT), S-velocity (from DTS), and density (Rho-b) are generally the minimum requirements for inversion to acoustic and shear impedances and estimation of rock properties. At the time of this study, 18 wells have been drilled in the area; however, only four (Acae 11, 10, 9, and 5, as shown in Figure 4) have a sufficient suite of logs through an appropriate well section to be used in the analysis. None of the wells was logged for DTS. Most well logs were of mixed quality and required significant editing.

The observed well bore condition in Acae 11, 9, and 5

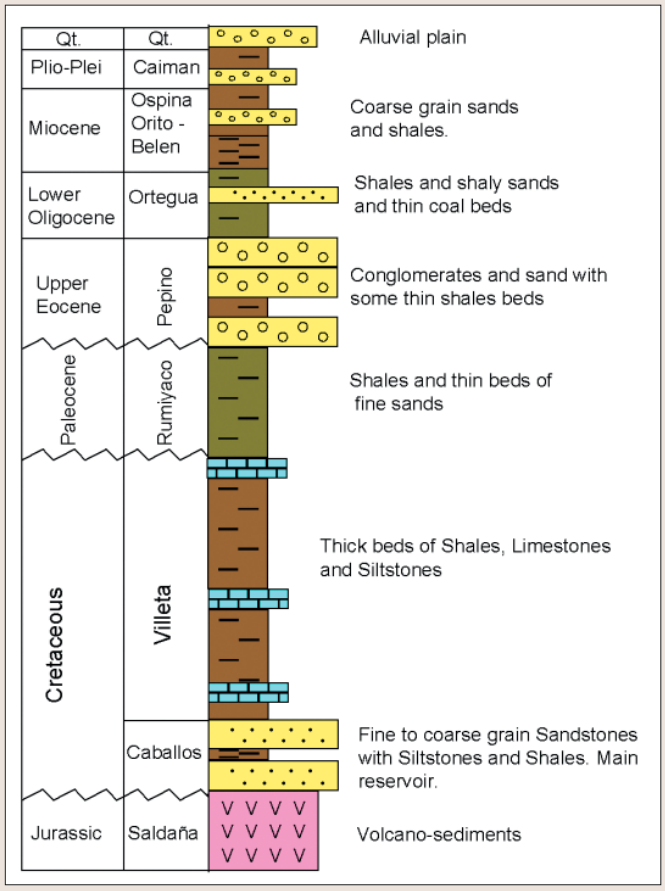

Figure 3. *Generalized stratigraphic sequence. (Figure modified from Peña et al., 2000.)*

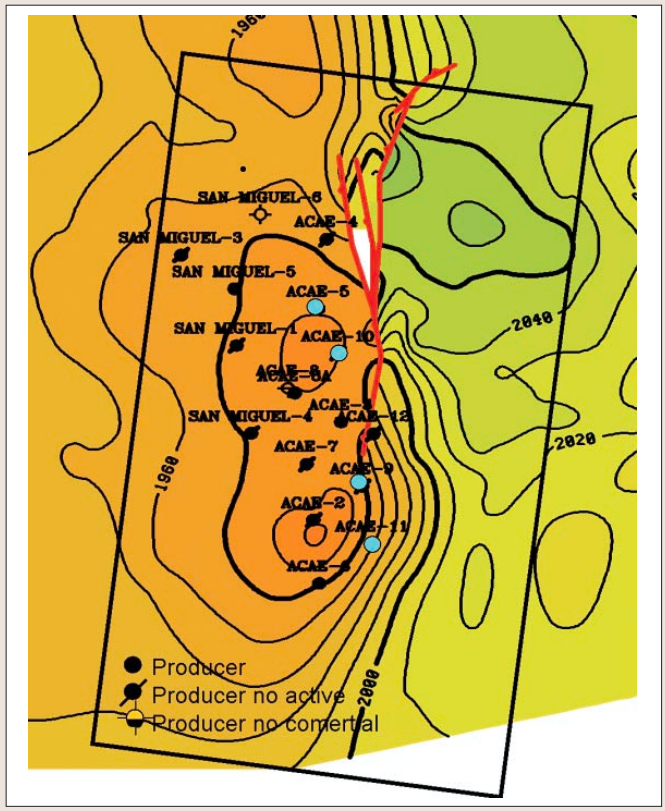

Figure 4. *Structural map at the top of the reservoir showing locations of wells Acae 11, 9, 10, and 5. The outlined area represents the 3D volume used in this study.*

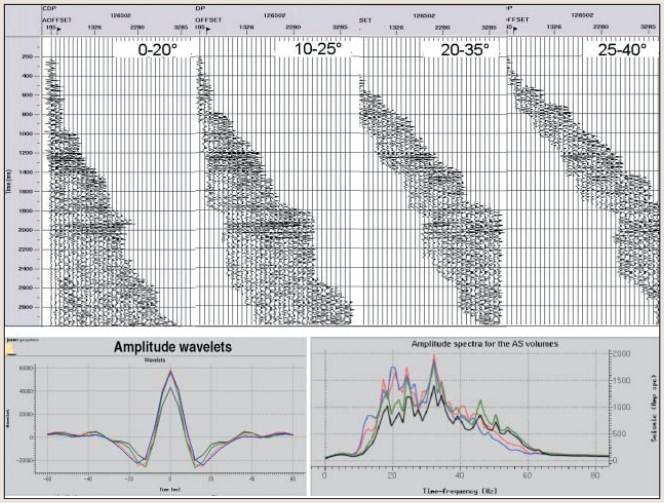

Figure 5. *(Top) Examples of partial-angle CDP gathers. (Bottom) Wavelets and amplitude spectra of the different ASVs. 0-20° (black), 10-25° (green), 20-35° (red), and 25-40° (blue).*

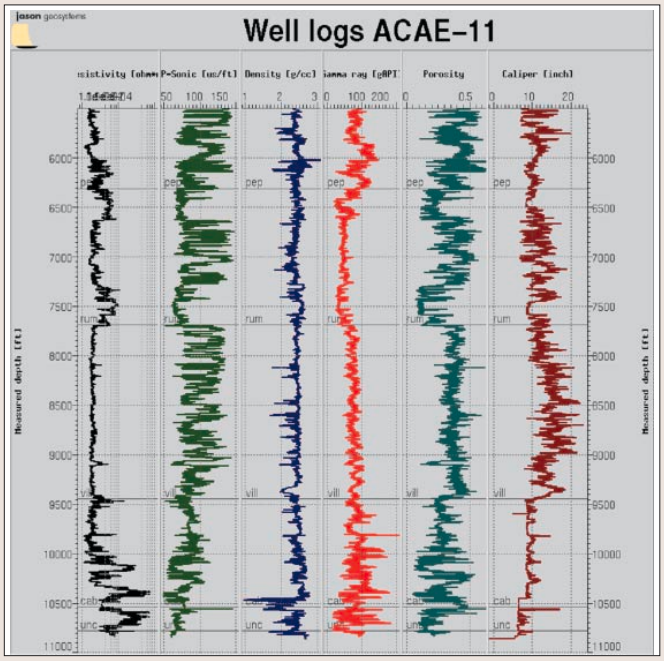

Figure 6. *Set of logs available from well Acae 11. From left to right: deep induction resistivity (R_{ILD}), P-sonic (DT), density (Rho-b), gamma ray (GR), neutron porosity (ϕ_N), and caliper. Core data are available for Caballos Formation from this well and from Acae 10. The caliper log indicates poor condition of the wellbore, implying that the log data for Rho-b, ϕ_N= and P-sonic are unreliable, and require significant editing.*

is very poor through Pepino and Rumiyaco formations (Figure 6). Although there are no exploration targets in those sections, it is necessary to have reliable log data through a sufficient section in order to carry out the seismic inversion and interpretation. The editing of the P-sonic log for cycle skipping at Pepino and Rumiyaco formations was conducted independently through the relationship between DT and conductivity (Figure 7), following a method similar to the one described by Burch ("Log ties seismic to ground truth" in the *AAPG Explorer*, February and March, 2002). The relationship was estimated initially in the Acae 10 where the well bore condition is good and little editing is required. Most problems with the DT log in Acae 11 appear due to cycle skipping and stretch, which always result in a longer DT (see the DT-conductivity crossplots in Figure 7).

In order to estimate total porosity (ϕ_t), we first obtained

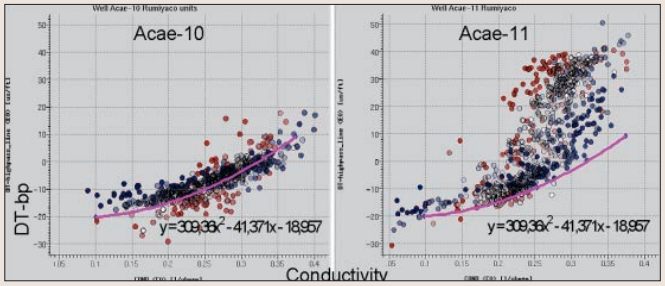

Figure 7. Crossplot of conductivity versus DT-bp or (DT bandpass filtered, in depth,removing the general trend related to depth of burial), for the Rumiyaco Formation. The relationship, shown by the colored line, was estimated at well Acae 10 (the well with best borehole conditions) in the left figure, and applied at wells Acae 11 (in the right figure, where the dots are shifted down to the line, correcting for cycle-skipping and DT stretch) and at wells Acae 9 and 5. Figure 11 shows the correction applied to the log trace of Acae 11.

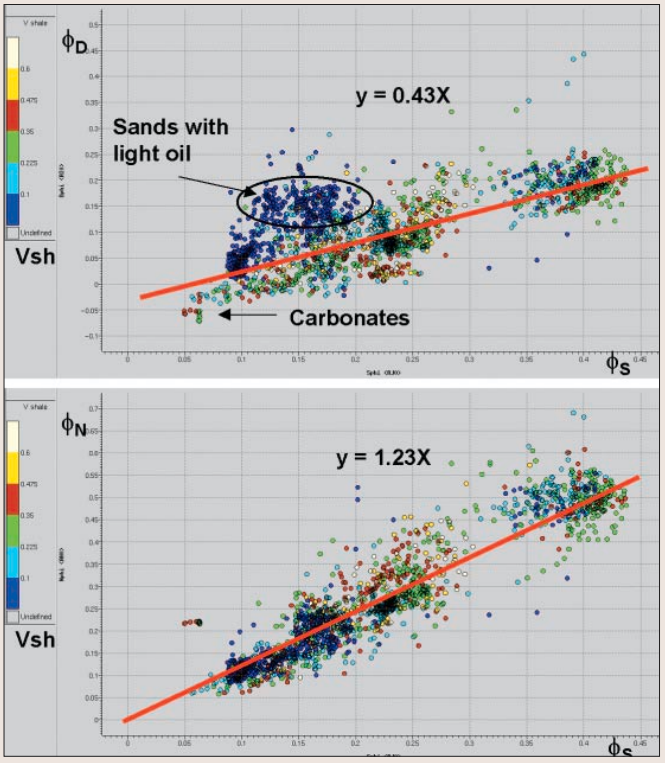

Figure 8. Relationships between ϕ_S with ϕ_D and ϕ_N for well Acae 11. Only data in zones of good borehole conditions were considered. The relationship was then applied to those zones with wash outs. The crossplots are colored by Vshale, where dark blue represents clean sand.

Figure 9. Track 1: Caliper log. Track 2: ϕ_N original (green) and calculated (light blue). Track 3: fD original (green) and calculated (black). Track 4: The final effective porosity was estimated from core data at the Caballos Formation (black, at deepest interval only), from original logs in zones with good borehole conditions (green) and from the calculated logs in the washout zones (blue).

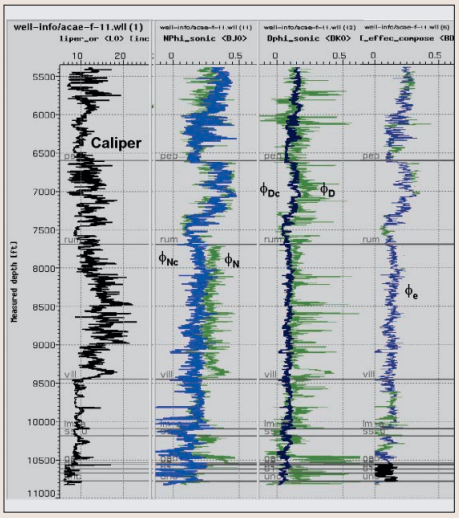

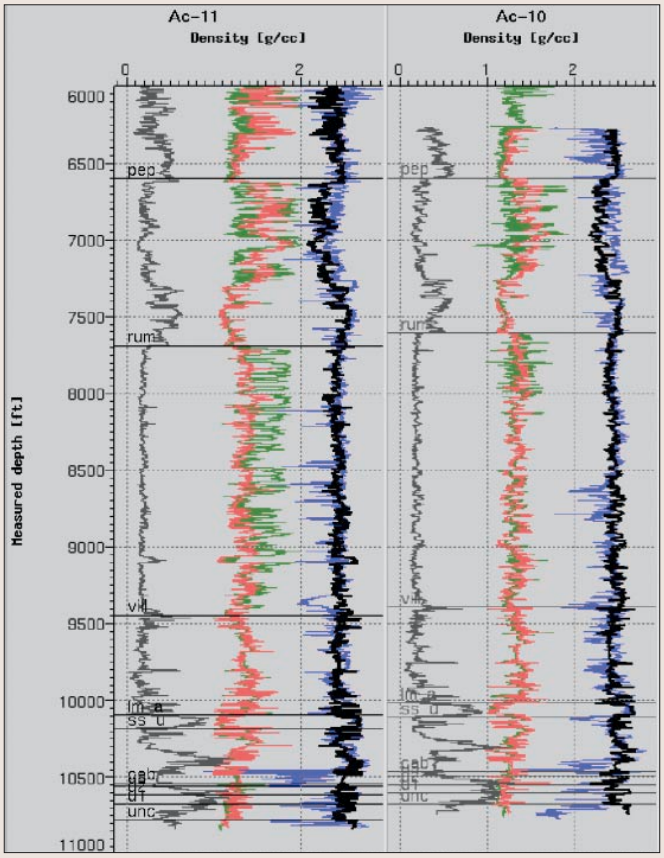

Figure 10. Corrections applied to P-sonic and Rho-b for the Acae 11 and Acae 10 wells. The scale is appropriate for density, and other logs are scaled for convenient display. From left to right: R_{ILD} (black, logarithmic scale) for reference; DT original (green) and DT calculated (red); Rho-b original (light blue) and calculated (dark blue).

relationships between the porosity derived from the sonic log (ϕ_S) and the porosities derived from the neutron and density logs (ϕ_N and ϕ_D, respectively), in those zones exhibiting good borehole conditions (Figure 8). These relationships were then extended to those zones with washouts or other problems. For Caballos Formation, the porosity log corrections were based on core laboratory measurements at Acae 11 and 10. We then applied conventional log-analysis procedures (e.g., Practical Formation Evaluation, 1995) to compute effective and total porosities from the corrected ϕ_N and ϕ_D logs because these parameters are useful for formation evaluation. Figure 9 is an example of the porosity logs before and after editing. Bulk density (for synthetic seismogram computation and inversion) was then computed from the porosity and the density of the matrix and fluid components, where the fluid properties were computed using the Batzle and Wang method, and based on formation test and PVT analysis. Figure 10 shows the correction in the well logs.

Measurements of shear velocity from full-waveform or dipole sonic logs were not available for this project, and we were forced to develop a synthetic relationship with other rock parameters. The Acae well data (Figure 11) show a clear association between porosity and V_P for rocks ranging from clean sandstones (blue dots) through shaly sandstones (green) to shale (yellow), represented schematically by the orange trend lines. Han (1986), Xu and White (1995), and Vernik (1998), among others, have observed similar trends for siliciclastic rocks. The Xu and White method to predict V_S exploits the V_P-porosity pattern shown in the log data. In addition, laboratory measurements of V_S in dry frame on core data from Acae 10 and Acae 8A (for clean sand)

compare favorably with Han et al. results for shear modulus versus porosity. These arguments provide us with confidence that the Xu and White approach will result in accurate Vs estimation and allow us to account for the varying clay content of the rocks and for the presence of water or water-and-oil in the pore space. The brine and live-oil bulk moduli were estimated using the Batzle and Wang method. The approach implemented here predicts V_P from other parameters as well as V_S, enabling calibration of the variables used in the Xu and White approach. The V_P predicted in our final model agrees quite closely with the logged (and edited) V_P data, giving us confidence in the calculated V_S log (Figure 12).

All corrections and calculations were applied in the same way for the four wells used to aid in the inversion process.

Seismic inversion process. A simultaneous AVA CSSI (amplitude variation with angle constrained sparse-spike inversion) process was performed in this study. The basis for the method was presented by Fullagard (1985) and Deveye and Van Riel (1990); extensions to the elastic impedance and simultaneous inversion concepts were described by Connolly (1999) and Pendrel et al. (2000), respectively.

Using Zoeppritz's, equation, four sets of EI logs were estimated for the wells Acae 11, 10, and 5; each ASV covered 15-20° in incident angles, with some overlap between neighboring ranges. EI logs for Acae 9 were not estimated; this well will be compared with the inversion results at its location, as a form of quality checking. Each ASV and the corresponding EI set of logs were used to estimate the corresponding wavelets, which were similar to the initially computed wavelets (shown in Figure 5), but with a small nonzero-phase component for the offset ASVs. The good match between the seismic traces around Acae 10 in an ASV and the synthetic traces generated with the corresponding wavelet indicates that the rock physics model used to correct the logs appears consistent with the seismic data (a near-angle example is shown in Figure 13).

Figure 14 shows the final results for band-limited P-impedance, S-impedance, and density from the seismic inversion process, and the correlation of those values with the well-log data at the four wells, including Acae 9 which was not used in the inversion. The results are very good, and we consider this inversion to have been quite robust, particularly for a three-term inversion. The final step in this inversion process involves merging with a low-frequency volume created by interpolating low-pass filtered log data along tracked horizons. Our final inversion result consists of three volumes (Figure 15): P-impedance, S-impedance, and density, which are then interpreted for rock quality; in this case, the rock quality was largely a function of shale content, and, in the clean sands, the mean porosity. These properties were inferred from the inverted P- and S-impedance and density volumes within the target interval, Caballos Formation.

The calculation of the mean porosity within Caballos Formation was based on the observed relationship between P-impedance and porosity (Figure 16). The following equation describes the procedure:

$$\phi = \sum_{i=1}^{n} \phi(\Delta z_i) \times \Delta t \times Vp(z_i) / 2n \qquad (1)$$

where:
$\phi(\Delta z_i)$ = function converting P-impedance in ϕ values, using the trend line for clean sands in Figure 16.
Δt = sample rate (4 ms)
$V_P(z_i)$ = function converting P-impedance into true interval velocity, using a trend line that takes into account an average density value for the Caballos section.
z_i = P-impedance value from the volume at each sample within the Caballos.
n = Number of P-impedance samples in the measure section.

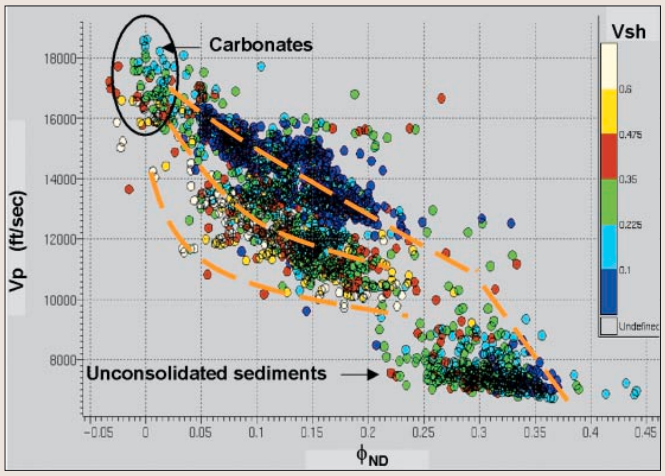

Figure 11. Relationship V_P - Porosity - Lithology at well Acae 11, from the original (not calculated) logs for intervals with good caliper conditions through the entire depth range. Color coding indicates Vshale determined from GR, and shows a strong dependence of the relationship on lithology, from clean sands (blue) to shale (light yellow).

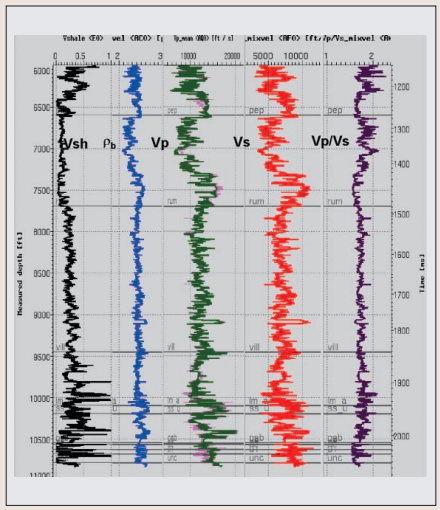

Figure 12. Final set of logs to be used during the inversion process and interpretation for well Acae 11. In the third track the original V_P log after P-sonic corrections (green) can be compared with the synthesized V_P log using the Xu and White approach (magenta). The error between the logs is 6%.The shear log associated with this model is shown in the fourth track (red), and the V_P/V_S ratio follows.

The mean porosity, assuming the entire Caballos Formation consists of clean sand, was found to vary laterally between approximately 11 and 14% (Figure 17), in agreement with porosity values at the wells from logs and core. The highest porosities are distributed in a region trending from the upper Caballos in the northwest to the lower Caballos in the southeast. V_P/V_S varies with the shaliness of the sand within this porosity range in a manner that allows a simple discrimination between clean sands and shaly sands, using either a polygon drawn on a crossplot of P-impedance versus S-impedance or a simple V_P/V_S cutoff; in this study, we used the polygon approach. From Figure 18 we can see that clean sand with good porosity is in the central and northwestern parts of the study area, including at least 70% of the reservoir zone.

Conclusions. Although the logs for Acae Field were poor due to borehole conditions, the methodology implemented for well-log editing allowed us to construct a complete suite

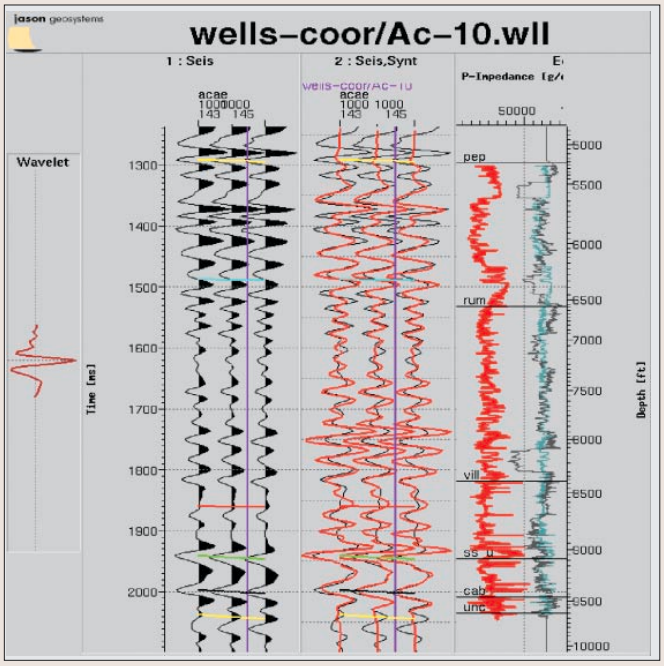

Figure 13. DTC result at well Acae 10. It is possible to see the good match between synthetic traces (red in track 3) and seismic traces (black in tracks 2 and 3) for the 0-20° ASV around the well. The wavelet used is shown at the left. To the right are displayed the logs for P-impedance (red), DT (cyan) and time (black, showing the extent of stretching and squeezing applied to obtain a quality fit). Similar ties were observed for the other wells.

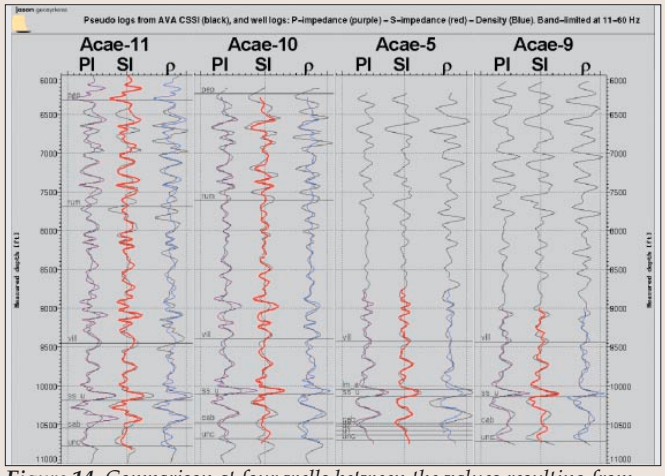

Figure 14. Comparison at four wells between the values resulting from seismic inversion for band-limited P-impedance (purple), S-impedance (red) and density (blue), and the corresponding values for the edited (P-impedance and density) or synthetic (S-impedance) well logs (black). All the values have a 10-60 Hz bandwith.

through the depth range required for inversion. Shear logs were synthesized using a single internally consistent rock physics model which was consistent with the shear impedances obtained from seismic inversion. The good correlation between the P-impedance, S-impedance, and density values as a product of the seismic inversion process, and the same values in the well-log data, strongly suggest that the changes in AVA in the seismic data are caused by changes in rock properties and not by processing or inversion artifacts.

The P-impedance values obtained through inversion for Caballos Formation are more closely related to porosity than to lithology. The mean porosity varies laterally and vertically between 11 and 14%, and these values agree with well logs and core data values.

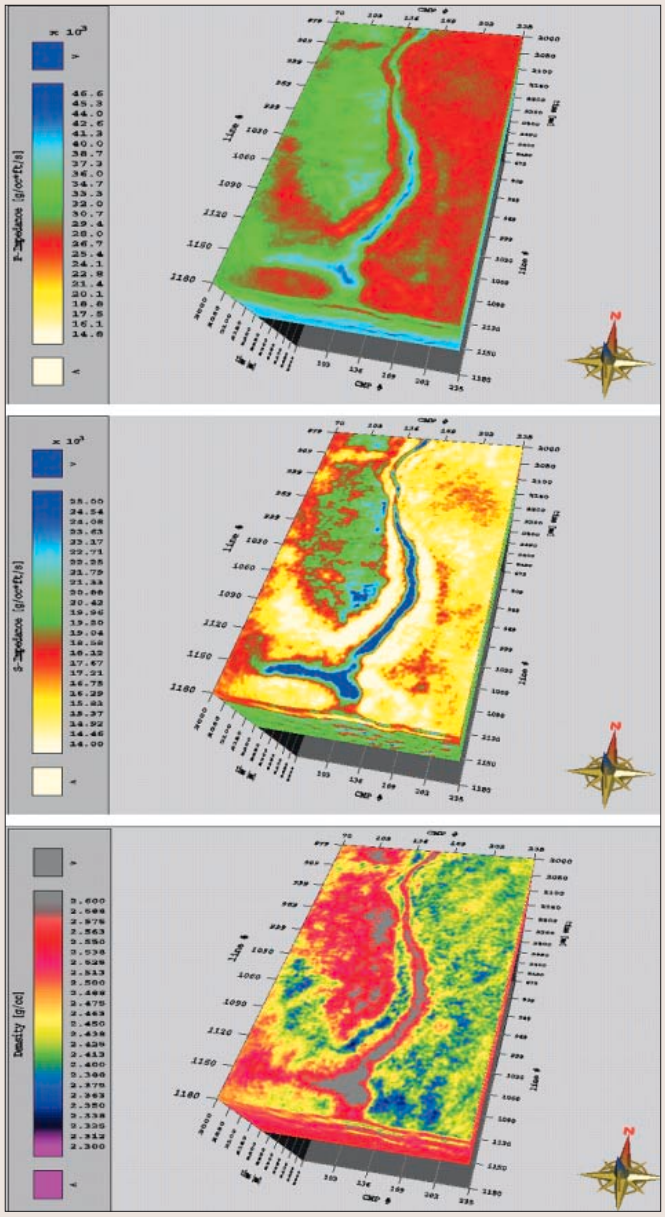

Figure 15. Time slices at the reservoir zone of the resulting volumes for absolute P-impedance (above), S-impedance (middle) and density (below). From north to south it is easy to follw the fault that limits the reservoir, which is located at the west.

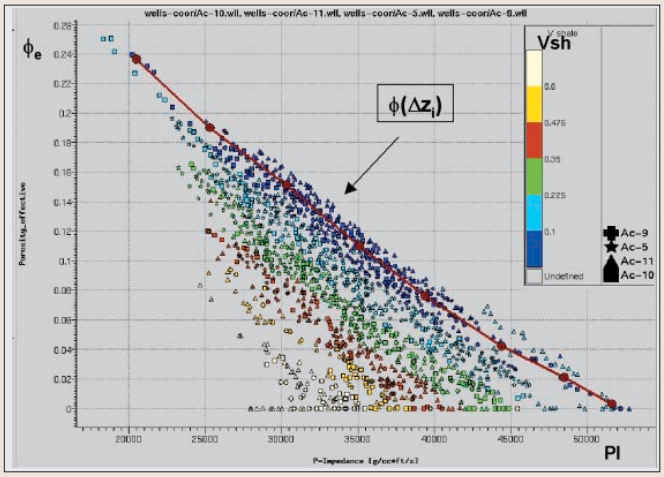

Figure 16. ϕ_e as a function of P-impedance for all four wells, colored by Vsh, where dark blue corresponds to clean sand.

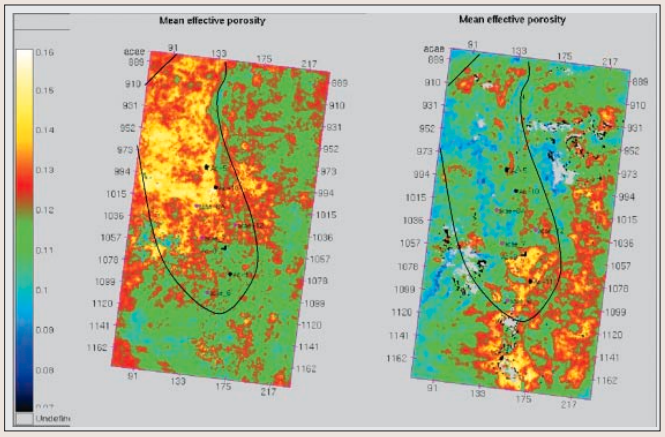

Figure 17. *Mean porosity in the upper (left) and lower (right) Caballos Formation.The black line represents the reservoir area, corresponding roughly to the oil-water contact.*

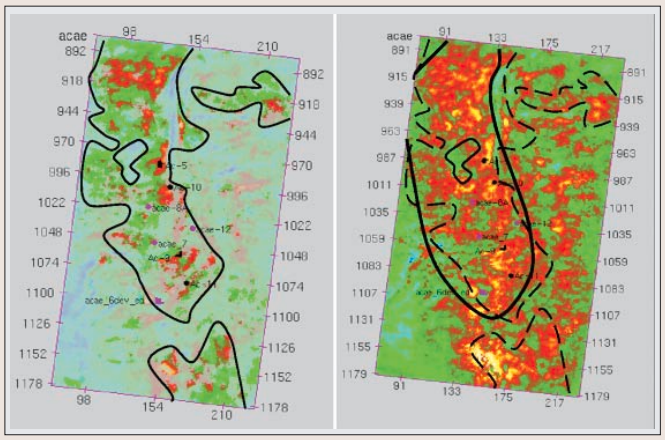

Figure 18. *Caballos Formation rock quality. Left: clean sands appear as the brighter values of P-impedance, which varies from low (yellow to red) to high (green to blue). Right: mean porosity through the entire Caballos Formation interval; fine contours are taken from the clean sand map to the left and the coarse contour indicates the reservoir area.*

V_P/V_S obtained from inversion was related to lithology. The porosity and V_P/V_S results, together, indicate that the best sand bodies for hydrocarbon accumulation are in the central and northwestern parts of the study area portion of the Puerto Colón oil field.

Suggested reading. "Seismic properties of pore fluid" by Batzle and Wang (GEOPHYSICS, 1992). "Log ties seismic to ground truth" by Burch (*AAPG Explorer*, 2002). "Elastic impedance" by Connolly (*TLE*, 1999). "Lp-norm deconvolution" by Debeye and van Riel (*Geophysical Prospecting*, 1990). "Spike recovery deconvolution" by Fullegar (in *Developments in Geophysical Exploration Method, Volume 6*, Elsevier, 1985). "Effects of porosity and clay content on wave velocity in sandstones" by Han et al. (GEOPHYSICS, 1986). "Estimation and interpretation of P- and S-impedance volumes from simultaneous inversion of P-wave offset seismic data" by Pendrel et al. (*SEG 2000 Expanded Abstracts*). "The acoustic log—principles and limitations" by Ransom (in *Practical Formation Evaluation*, John Wiley & Sons, 1995). "A new velocity model for clay-sand mixtures" by Xu and White (*Geophysical Prospecting*, 1995). "How to obtain reliable S-impedance from P-wave data" by Cambois (*World Oil*, 2001). "Shear-wave velocity estimation in porous rocks: Theoretical formulation, preliminary verification, and application (*Geophysical Prospecting*, 1992). TLE

Corresponding author: horacio.acevedo@ecopetrol.com.co